BIOCHEMISTRY
including biophysical chemistry & molecular biology

Article

pubs.acs.org/biochemistry

Ionic Residues of Human Serum Transferrin Affect Binding to the Transferrin Receptor and Iron Release

Ashley N. Steere,[†] Brendan F. Miller,[†] Samantha E. Roberts,[†] Shaina L. Byrne,[†,∥] N. Dennis Chasteen,[‡] Valerie C. Smith,[§] Ross T. A. MacGillivray,[§] and Anne B. Mason*[,†]

[†]Department of Biochemistry, University of Vermont, College of Medicine, 89 Beaumont Avenue, Burlington, Vermont 05405, United States

[‡]Department of Chemistry, Parsons Hall, University of New Hampshire, Durham, New Hampshire 03824, United States

[§]Department of Biochemistry and Molecular Biology and Centre for Blood Research, University of British Columbia, Vancouver, BC V6T 1Z3, Canada

Supporting Information

ABSTRACT: Efficient delivery of iron is critically dependent on the binding of diferric human serum transferrin (hTF) to its specific receptor (TFR) on the surface of actively dividing cells. Internalization of the complex into an endosome precedes iron removal. The return of hTF to the blood to continue the iron delivery cycle relies on the maintenance of the interaction between apohTF and the TFR after exposure to endosomal pH (≤6.0). Identification of the specific residues accounting for the pH-sensitive nanomolar affinity with which hTF binds to TFR throughout the cycle is important to fully understand the iron delivery process. Alanine substitution of 11 charged hTF residues identified by available structures and modeling studies allowed evaluation of the role of each in (1) binding of hTF to the TFR and (2) TFR-mediated iron release. Six hTF mutants (R50A, R352A, D356A, E357A, E367A, and K511A) competed poorly with biotinylated diferric hTF for binding to TFR. In particular, we show that Asp356 in the C-lobe of hTF is essential to the formation of a stable hTF−TFR complex: mutation of Asp356 in the monoferric C-lobe hTF background prevented the formation of the stoichiometric 2:2 (hTF:TFR monomer) complex. Moreover, mutation of three residues (Asp356, Glu367, and Lys511), whether in the diferric or monoferric C-lobe hTF, significantly affected iron release when in complex with the TFR. Thus, mutagenesis of charged hTF residues has allowed identification of a number of residues that are critical to formation of and release of iron from the hTF−TFR complex.

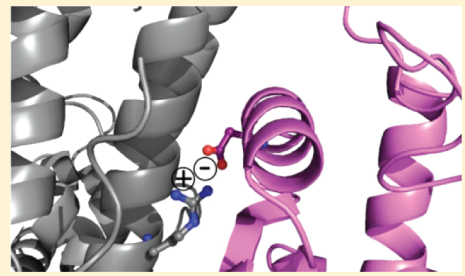

The transport of iron throughout the body by human serum transferrin (hTF) is central to iron homeostasis. The homologous N- and C-lobes of hTF are divided into two subdomains (N1 and N2, C1 and C2) that fold to form a deep cleft capable of binding a single ferric iron. Sequestration of highly insoluble Fe^{3+} by hTF maintains iron in the blood in a nonreactive state, preventing reduction to ferrous iron (Fe^{2+}) that can catalyze the production of reactive oxygen species via Fenton chemistry. Four unequally distributed species of hTF differing with regard to iron content are found in plasma: diferric hTF, monoferric N-lobe hTF, monoferric C-lobe hTF, and apohTF (iron-free).[1−3] Physiologically, one molecule of hTF binds tightly to each monomer of the homodimeric transferrin receptor (TFR) located on the extracellular surface of dividing cells. A transmembrane glycoprotein, each TFR monomer is composed of three domains: a helical domain responsible for dimerization, an apical domain, and a protease-like domain.[4]

At pH 7.4, the TFR preferentially binds diferric hTF (with low nanomolar affinity), the two monoferric hTFs bind ∼10-fold weaker, and apohTF binds very weakly, if at all.[5] Within the endosome, following clathrin-dependent endocytosis of the hTF−TFR complex and upon exposure to a slightly more acidic pH, hTF releases Fe^{3+} to an unidentified chelator in a TFR-mediated process. Large conformational changes in each lobe are associated with opening of the cleft and iron release.[6] In spite of these large conformational changes, apohTF remains bound to the TFR at the mildly acidic pH (∼5.6) of the endosome, implying that the binding partners accommodate and compensate for these structural changes.[7] Essential to the hTF cycle, the apohTF−TFR complex is recycled back to the cell surface, whereupon exposure to the neutral pH of blood, apohTF is released from the TFR and is free to sequester more iron.

Mapping the hTF−TFR interface has been hampered by a lack of structural data for the complex. A 7.5 Å resolution cryo-electron microscopy (cryo-EM) model of TF and the extracellular portion of the TFR provided the first view of the complex.[8] The model indicated that the N-lobe is situated between the membrane and the TFR, while the C-lobe makes significant contacts with the helical domain of the TFR [Protein

Received: November 3, 2011
Revised: December 21, 2011
Published: December 22, 2011

Data Bank (PDB) entry 1SUV]. However, given the relatively low resolution, as well as the requirement of an ~9 Å shift to place the N-lobe of hTF into the density,[8] the model lacked the precision needed to identify specific interactions between hTF and the TFR. More recently, the availability of the apohTF structure[6] and consideration of results from mutagenesis studies of both hTF and the TFR led to in silico models of both diferric hTF and apohTF bound to the TFR.[9] Significantly, these models eliminated the need for the 9 Å gap between the N- and C-lobes of hTF. Because of their ability to serve as stabilizing forces in promoting nanomolar binding affinity, identification of the ionic interactions between hTF and the TFR was a major focus of both studies. The cryo-EM model of the hTF−TFR complex predicted a network of four salt bridges between the C1 subdomain of hTF and the helical domain of the TFR.[8] Although not specific with regard to precise interacting partners, residues from the hTF C1 subdomain (including Asp356, Glu357, Glu367, and Glu372) were predicted to interact strongly with the TFR through the formation of salt bridges.

The in silico model, based mainly on the cryo-EM model, proposed a number of specific ionic interactions between residues of hTF (Table 1) and the TFR, along with two of the hTF residues previously identified in the cryo-EM model, Glu357 and Glu367.[9] However, the newly available high-resolution (3.22 Å) X-ray crystal structure of recombinant monoferric N-lobe hTF (Fe_NhTF) and the soluble portion of the TFR (sTFR, residues 121−670) identified only one salt bridge in each lobe of hTF: between Arg50 in the N1 subdomain of hTF and Glu664 in the sTFR (Figure 1A) and between Asp356 in the C1 subdomain of hTF and Arg651 in the sTFR (Figure 1D).[10] Additionally, the location of hTF α-helix 1, on which both Asp356 and Glu357 are found, was shifted by nearly 5 Å (approximately one full helical turn) in the Fe_NhTF−sTFR structure as compared to the cryo-EM model,[10] possibly invalidating some of the binding partners predicted by the in silico model.

Table 1. Proposed Ionic Interactions between hTF and the TFR

hTF residue	hTF subdomain (secondary structure)	TFR residue	TFR domain (secondary structure)	refs
Arg50	N1 (α-helix 2)	Glu664	helical (loop 663−667)	10[a]
Glu141	N2 (loop 139−145)	Lys508	protease-like (helix αI-7)	9[b]
Lys148	N2 (α-helix 6)	Asp125/Asp126	protease-like (helix αI-1)	9, 10
Glu333	bridge (residues 332−338)	Lys508	protease-like (helix αI-7)	9
Arg352	C1 (α-helix 1)	Ser644-Gly647-Asp648	helical (helix αIII-3)	9
Asp356	C1 (α-helix 1)	Arg651	helical (helix αIII-3)	10
Glu357	C1 (α-helix 1)	Arg629/Tyr643	helical (helix αIII-2)/helical (helix αIII-3)	9, 10
Glu367	C1 (β-strand 2)	Arg646/Phe650	helical (helix αIII-3)	9, 10
Glu385	C1 (loop 384−387)	Arg651	helical (helix αIII-3)	9
Lys511	C2 (loop 505−515)	Glu759	helical (C-terminus)	9
Glu625	C1 (loop 609−636)	Lys633	helical (helix αIII-2)	9

[a]Structure of the Fe_NhTF−sTFR complex.[10] [b]The in silico model of Sakajiri et al.[9] was based on the cryo-EM model[8] in conjunction with available mutagenesis data.

Given the dramatic effect of the TFR on the release of iron from hTF (increasing the rate of release of iron from the C-lobe of hTF by 7−11-fold and decreasing the rate of release of iron from the N-lobe by 6−15-fold),[11] identification of the contacts between the two proteins is clearly critical. The structural features that confer the ability of the TFR to bind hTF at both acidic and neutral pH while accommodating the significant conformational changes that take place during the process of iron release require further investigation. The proposed ionic interactions between hTF and the TFR from the cryo-EM model, from the in silico model, and from our crystal structure of the Fe_NhTF−sTFR complex are summarized in Table 1. Many of the TFR residues listed in Table 1 have been mutated and investigated with regard to their effect on binding of both diferric hTF and apohTF using surface plasmon resonance.[12] We have taken the complementary approach of mutating the residues in hTF (Arg50, Glu141, and Lys148 in the N-lobe, Glu333 in the bridge between the two lobes, and Arg352, Asp356, Glu357, Glu367, Glu385, Lys511, and Glu625 in the C-lobe) proposed to form ionic interactions with the TFR (Figure 1 of the Supporting Information).

MATERIALS AND METHODS

Materials. Dulbecco's modified Eagle's medium-Ham F-12 nutrient mixture, antibiotic-antimycotic solution (100×), fetal bovine serum, and trypsin were from the Gibco-BRL Life Technologies Division of Invitrogen. Ultroser G is a serum replacement from Pall BioSepra (Cergy, France). Methotrexate from Bedford Laboratories was purchased at a local hospital pharmacy. The QuikChange mutagenesis kit was from Stratagene. All tissue culture dishes, flasks, and Corning expanded surface roller bottles were from local distributors. Ultracel 30 kDa molecular mass cutoff (MMCO) membrane microconcentrator devices were made by Amicon. Ni-nitrilotriacetic acid (NTA) resin was from Qiagen. Hi-prep 26/60 Sephacryl S-200HR and S-300HR columns were acquired from Amersham Pharmacia. Ethylenediaminetetraacetic acid (EDTA) was from Mann Research Laboratories, Inc. NTA and ferrous ammonium sulfate were from Sigma. Novex 6% tris(hydroxymethyl)aminomethane−borate−EDTA (TBE) urea minigels, TBE running buffer (5×), and TBE−urea sample buffer (2×) were from Invitrogen. The 3,3′,5,5′-tetramethylbenzidine (TMB) microwell peroxidase (one-component) substrate system was from Kirkegaard and Perry Laboratories (Gaithersburg, MD). The A4A6 monoclonal antibody to the TFR was a generous gift from the laboratory of J. Cook at the University of Kansas Medical Center (Kansas City, KS). Removawells (Immulon 1B) were from Thermo Scientific.

Expression and Purification of Charged Residue-to-Alanine hTF Mutants. All mutations were introduced into the pNUT vector containing the cDNA encoding Fe_2hTF (recombinant N-terminally hexa-His-tagged nonglycosylated diferric hTF) or Fe_ChTF [recombinant N-terminally hexa-His-tagged nonglycosylated monoferric hTF that binds iron only in the C-lobe (Y95F and Y188F mutations prevent iron binding in the N-lobe)] using the QuikChange site-directed mutagenesis kit as previously described.[13] Forward mutagenic primers used to introduce the hTF mutations are shown below. The

dx.doi.org/10.1021/bi201661g | Biochemistry 2012, 51, 686−694

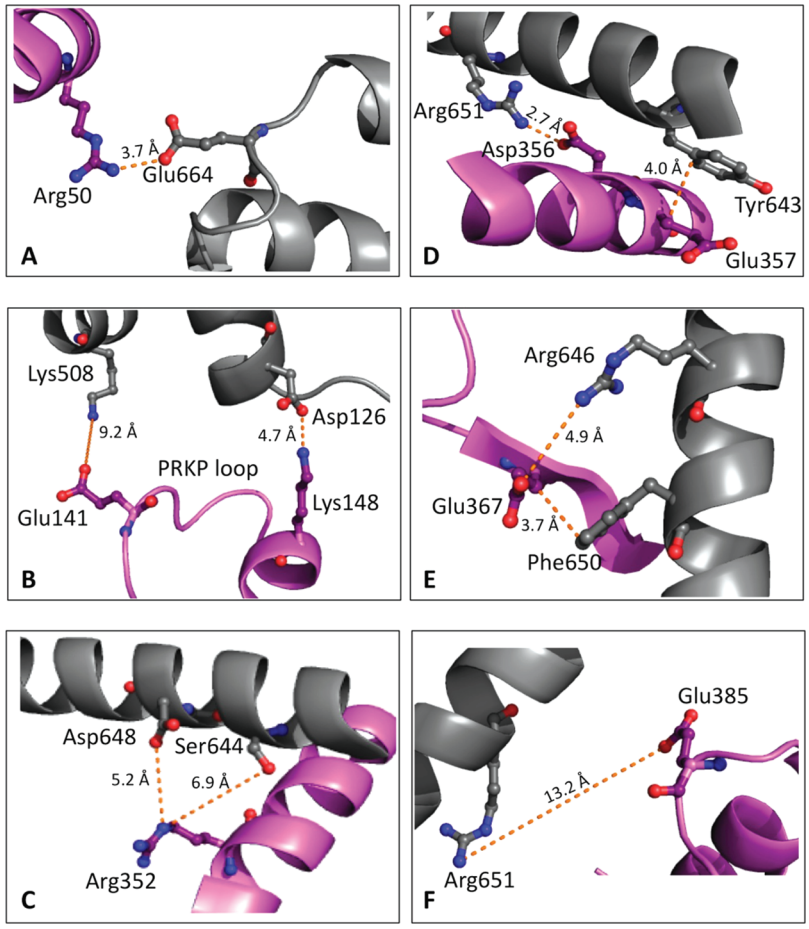

Figure 1. Location of charged hTF residues in the Fe_NhTF−sTFR crystal structure (PDB entry 3S9L).[10] hTF residues (A) Arg50, (B) Glu141 and Lys148, (C) Arg352, (D) Asp356 and Glu357, (E) Glu367, and (F) Glu385 are colored purple. Residues in the sTFR proposed to interact with the charged hTF residues (Table 1) are colored gray. This figure was generated using PyMOL.[18]

substitutions resulting in the mutations are underlined and bold: R50A, 5′ CC TAC CTT GAT TGC ATC **GC**G GCC ATT GCG GCA AAC G 3′; E141A, 5′ T TAC TGT GAC TTA CCT G**C**G CCA CGT AAA CCT CTT G 3′; K148A, 5′ GAG CCA CGT AAA CCT CTT GAG **GC**A GCA GTG GCC 3′; E333A, 5′ GGC ACA TGC CCA G**C**A GCC CCA ACA GAT GAA TGC 3′; R352A, 5′ G CTG AG**T** CAC CAC GAG **GC**G CTC AAG TGT GAT GAG 3′; D356A, 5′ GG CTC AAG TGT G**C**T GAG TGG AGT GTT AAC AGT GTA GGG 3′; E357A, 5′ GG CTC AAG TGT GAT G**C**G TGG AGT GTT AAC AGT GTA GGG 3′; E367A, 5′ AC AGT GTA GGG AAA ATA G**C**G TGT GTA TCA GCA GAG AC 3′; E385A, 5′ C AAG ATC ATG AAT GGA G**C**A GCT GAT GCC ATG AGC T 3′; K511A, 5′ C CTA AAC CTG TGT GAA CC**G** AAC AAC **GC**A GAG GGA TAC TAC 3′; E625A, 5′ TGT TTG TTC CG**C** TCG G**C**A ACC AAG GAC CTT CTG 3′.

Baby hamster kidney (BHK) cells were transfected with the pNUT plasmid encoding each of the mutants. Following expansion into expanded surface roller bottles, recombinant proteins were secreted into the tissue culture medium by the adherent BHK cells. All mutant hTFs were purified in their iron-saturated forms as previously described in detail.[14] Each purified hTF was concentrated to 15 mg/mL in 100 mM NH_4HCO_3 using a 30 kDa MMCO microconcentrator. Because the visible absorption maximum is indicative of the correct folding of the hTF and the geometry of the site, the UV−vis spectrum was recorded to determine the iron binding properties of each mutant. The production and purification of the His-tagged sTFR consisting of residues 121−760 were as previously described.[15]

The formation of hTF−sTFR complexes was accomplished by adding a small molar excess (~20%) of control or mutant hTF to 1.5 mg of sTFR. Following equilibration at room temperature for ~5 min, hTF−sTFR complexes were purified by passage over a Sephacryl S-300HR gel filtration column in 100 mM NH_4HCO_3 to separate excess hTF. Fractions with the complex were concentrated to 15 mg/mL with respect to hTF.

Solution-Based Competition Assay To Determine the Relative Binding Affinity of the Recombinant Fe_2hTF Mutants. The competitive immunoassay described in detail previously has been modified in our application.[16] Briefly, Removawells were coated with rabbit anti-mouse IgG (1 mg/100 mL) to capture a mAb (A4A6) specific to the sTFR. Approximately 40 ng of mAb was added to each well. Following incubation for 40−60 min at 37 °C, a solution of the sTFR containing 400 ng/well was added to saturate the mAb binding sites. Incubation as described above was followed by addition of a constant amount of biotinylated Fe_2hTF (20 ng/well) in the presence or absence of unlabeled Fe_2hTF standards and the mutants. A tube with no added unlabeled Fe_2hTF establishes the maximal amount of biotinylated hTF that can be bound to the sTFR (B_{100}), and wells with no added specific mAb determine the amount of biotinylated hTF that is nonspecifically bound (B_0). A standard curve was generated by

dx.doi.org/10.1021/bi201661g | *Biochemistry* 2012, 51, 686−694

competition of biotinylated hTF with six different amounts of unlabeled Fe_2hTF (16−400 ng/well). Following washing, an avidin−HRP conjugate was added to all wells. The amount of biotinylated Fe_2hTF sample bound to the sTFR was determined using a TMB substrate system. All steps were conducted in buffer composed of 50 mM Tris-HCl (pH 7.4) containing 100 mM NaCl and 0.1% bovine serum albumin (BSA). Between each step, incubations at 37 °C for 40−60 min are followed by at least three washes of 200 μL/well. The Fe_2hTF control and each of the mutants were made up to a concentration of 20 μg/mL, and aliquots were assayed to determine the concentration of each using the standard curve as described previously.[16]

Urea Gel Analysis of hTF Mutants. The iron status of the charged residue-to-alanine hTF mutants in the presence and absence of the sTFR was examined by urea gel electrophoresis using Novex 6% TBE−urea minigels in 90 mM Tris-borate (pH 8.4) containing 16 mM EDTA as previously described.[11,14] Iron-containing samples were mixed in a 1:1 ratio with 2× TBE−urea gel sample buffer (final concentration of 0.5 μg/μL). To determine the extent of removal of iron from the various hTF mutants, an aliquot of each was added to iron removal buffer [100 mM MES buffer (pH 5.6) containing 300 mM KCl and 4 mM EDTA] and incubated at room temperature (15 min for hTF samples and 5 min for hTF−sTFR samples). The iron removal process was halted by addition of 2× TBE−urea gel sample buffer. Samples (3.0 μg) were loaded, and the gel was electrophoresed for 2.25 h at 125 V. Protein bands were visualized by Coomassie blue staining.

Kinetic Analysis of the Release of Iron from hTF Mutants with or without the sTFR at pH 5.6. The release of iron from the charged residue-to-alanine hTF mutants was monitored at 25 °C as previously described using an Applied Photophysics SX.20MV stopped-flow spectrofluorimeter.[11,14] One syringe contained the hTF sample or hTF−sTFR complex (375 nM) in 300 mM KCl, and the other syringe contained MES buffer (200 mM, pH 5.6), KCl (300 mM), and EDTA (8 mM). Rate constants were determined by fitting the change in fluorescence intensity versus time using Origin (version 7.5) to standard models as described in detail previously.[11,14] All data were corrected to zero fluorescence intensity at time zero before fitting.

We have previously shown that the presence of the sTFR induces a switch in the order of iron release such that the majority (65%) of the time iron is first released from the C-lobe followed by the N-lobe ($k_{1C} \rightarrow k_{2N}$).[11] However, unlike in the absence of the sTFR, the alternative pathway (N-lobe → C-lobe, k_{1N} and k_{2C}) is utilized the remaining 35% of the time, necessitating its inclusion in the fits of the Fe_2hTF−sTFR data. Therefore, as described in detail previously,[11] independently obtained values for the alternative pathway (k_{1N} and k_{2C}) are held constant while the Fe_2hTF−sTFR data are fit to obtain values for the more frequently used pathway (k_{1C} and k_{2N}).

RESULTS

Relative Binding Affinity of the Fe_2hTF Mutants for the sTFR. To investigate the details of the hTF−TFR interactions, the relative binding affinities of the Fe_2hTF mutants for the sTFR were measured using a competitive assay (Figure 2). Importantly, no significant differences in the visible absorption maxima or spectral ratios were observed for any of the mutants in comparison to the values of the appropriate hTF controls (data not shown), indicating that the mutants were properly folded and that none of the mutations disturbed the geometry of the iron binding site. Each mutant was then tested for its ability to compete with biotinylated Fe_2hTF for binding to the sTFR (noncovalently immobilized to the A4A6 mAb). Unlabeled Fe_2hTF was used to create a standard curve and served as the control to which the mutants were compared. Only the E333A mutant was equal to the Fe_2hTF control in its ability to compete with Fe_2hTF for binding to the sTFR. Conversely, most of the mutations did not compete in an equivalent manner; i.e., the hTF mutation affected binding to the sTFR. Most notably, the D356A Fe_2hTF construct did not compete at all with biotinylated Fe_2hTF for binding to the sTFR in this format, highlighting the importance of this residue (Asp356) in the interaction between hTF and the TFR. A number of the other hTF mutations (R50A, R352A, E357A, E357A/E625A, E367A, and K511A) significantly affected the ability of the mutant to compete with Fe_2hTF (approximately one-third of the control or less), although to a lesser extent than the D356A mutant, while the remaining mutants (E141A, K148A, and E385A) were approximately half as effective as the control at binding to the sTFR. To provide context, neither monoferric hTF (Fe_NhTF or Fe_ChTF), each of which is known to bind ∼10-fold more weakly to the TFR than Fe_2hTF, was able to effectively compete with biotinylated Fe_2hTF for binding to the sTFR using this format (data not shown). This finding highlights the limited range of binding that can be detected by this assay.

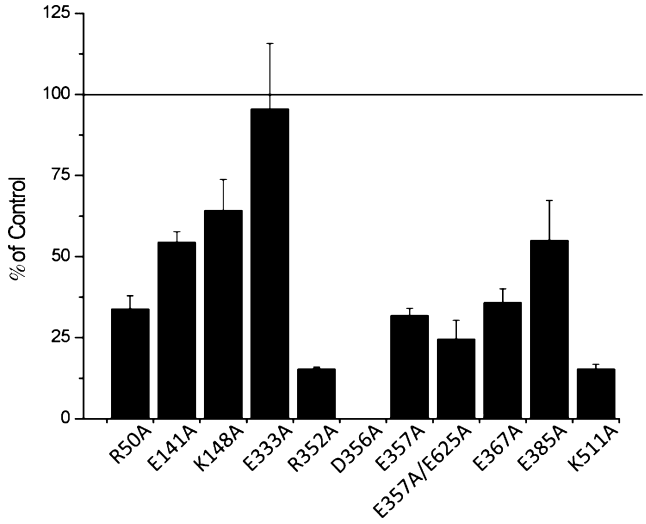

Figure 2. Evaluation of the abilities of single-point charged residue-to-alanine Fe_2hTF mutants to bind to the sTFR. All mutant hTF samples were prepared at a concentration of 20 μg/mL and competed with biotinylated Fe_2hTF for binding to immobilized sTFR. All values are expressed as a percentage of control (Fe_2hTF) binding and are averages of at least three different experiments ± the standard deviation.

Kinetic Analysis of Release of Iron from Fe_2hTF Mutants (in the absence of the sTFR). Kinetic rate constants for iron release at pH 5.6 obtained from the analysis of the Fe_2hTF control and the 11 charged residue-to-alanine hTF mutants in the absence of the sTFR are presented in Table 1 of the Supporting Information. Under our standard conditions [100 mM MES (pH 5.6) containing 300 mM KCl and 4 mM EDTA], the release of iron from Fe_2hTF produces two kinetic rate constants: rapid release of iron from the N-lobe (k_{1N}), followed by slow release of iron from the C-lobe (k_{2C}).[11]

dx.doi.org/10.1021/bi201661g | Biochemistry 2012, 51, 686−694

We have previously established that release of iron from Fe_2hTF proceeds through this pathway (N-lobe → C-lobe) 96% of the time, precluding the need to include the alternative pathway (C-lobe → N-lobe, k_{1C} and k_{2N}) in the fitting parameters.[11] As one might expect, in the absence of the sTFR, minimal differences are observed between the Fe_2hTF control and the hTF mutants (Table 1 and Figure 3 of the Supporting Information).

Kinetic Analysis of Release of Iron from Fe_2hTF Mutants (in the presence of the sTFR). Rate constants for the release of iron from Fe_2hTF and the charged residue-to-alanine Fe_2hTF mutants in the presence of the sTFR at pH 5.6 are reported in Table 2. In the presence of the sTFR, 4 of the 11 Fe_2hTF mutants (E141A, K148A, E333A, and E357A/E625A) had no significant effect on the release of iron from either lobe. Of the remaining mutants, the R50A, R352A, and E385A mutant Fe_2hTF–sTFR complexes exhibited slightly decreased rates of release of iron from the C-lobe (~27–44%), while release of iron from the N-lobe was essentially unchanged. Conversely, the E357A Fe_2hTF–sTFR and K511A Fe_2hTF–sTFR complexes caused the rate of release of iron from the C-lobe to increase slightly (36 and 47%, respectively). The most significant effect was observed in the D356A Fe_2hTF–sTFR mutant complex, which caused the rate of release of iron from the C-lobe to increase by ~133%. These results were substantiated by urea gel analysis, which confirms the iron status of the mutant complex. As shown in Figure 3, following a 5 min incubation in iron removal buffer [100 mM MES (pH 5.6) containing 300 mM KCl and 4 mM EDTA], little to no iron remained in the C-lobe of the D356A, E357A, and K511A Fe_2hTF mutants in the presence of the sTFR.

Table 2. Kinetics of Release of Iron from Charged Residue-to-Alanine Mutants in an Fe_2hTF Background in the Presence of the sTFR

	k_{1C} (min^{-1})	k_{2N} (min^{-1})
Fe_2hTF[a]	5.5 ± 0.9	1.4 ± 0.2
R50A Fe_2hTF	3.9 ± 0.2	1.6 ± 0.1
E141A Fe_2hTF	5.0 ± 0.8	1.6 ± 0.6
K148A Fe_2hTF	5.6 ± 0.7	1.5 ± 0.2
E333A Fe_2hTF	4.7 ± 0.8	1.9 ± 0.7
R352A Fe_2hTF	3.1 ± 0.6	2.0 ± 1.2
D356A Fe_2hTF	12.8 ± 0.7	1.5 ± 0.1
E357A Fe_2hTF	7.5 ± 0.8	1.1 ± 0.1
E367A Fe_2hTF	6.6 ± 1.0	–
E385A Fe_2hTF	4.0 ± 0.7	1.3 ± 0.2
K511A Fe_2hTF	8.1 ± 0.7	1.4 ± 0.2
E357A/E625A Fe_2hTF	4.9 ± 0.8	1.3 ± 0.1

[a]From ref 11. Rate constants for the other pathway are as follows: k_{1N} = 2.8 min^{-1}, and k_{2C} = 7.2 min^{-1}.

In contrast to the Fe_2hTF–sTFR control and the other Fe_2hTF mutant complexes, the E367A Fe_2hTF–sTFR complex fit to a simple A → B model providing only a single rate constant (Table 2 and Figure 4). Attempts to fit the data of the E367A Fe_2hTF–sTFR complex to various alternative models yielded poor fits (Figure 3 of the Supporting Information). The single rate constant obtained for the E367A Fe_2hTF–sTFR complex (k = 6.6 ± 1.0) is similar to the rate constant for the release of iron from the C-lobe of the Fe_2hTF–sTFR complex (k_{1C} = 5.5 ± 0.9). Therefore, it appears that the rate of release of iron from the N-lobe is significantly slowed such that the rate cannot be obtained from analysis of the data of the E367A Fe_2hTF–sTFR complex. The assignment of the single rate constant to release of iron from the C-lobe is supported by urea gel analysis of the E367A Fe_2hTF–sTFR complex in which all of the iron is removed from the C-lobe and an enrichment of Fe_NhTF is observed (Figure 3).

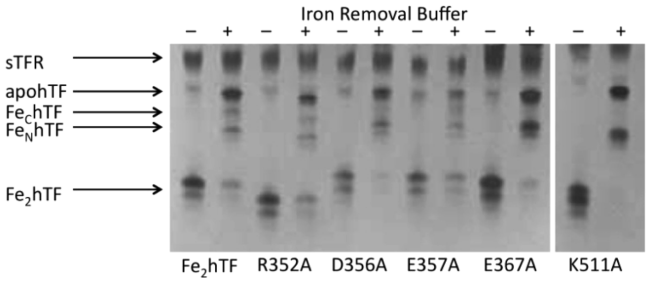

Figure 3. Urea gel analysis of selected charged residue-to-alanine Fe_2hTF mutants in the presence of the sTFR. Samples were electrophoresed before (–) and after (+) incubation with iron removal buffer [100 mM MES (pH 5.6) containing 300 mM KCl and 4 mM EDTA] for 5 min. Note the migration patterns of the charged residue-to-alanine mutants differ from that of Fe_2hTF because of differences in overall surface charge.

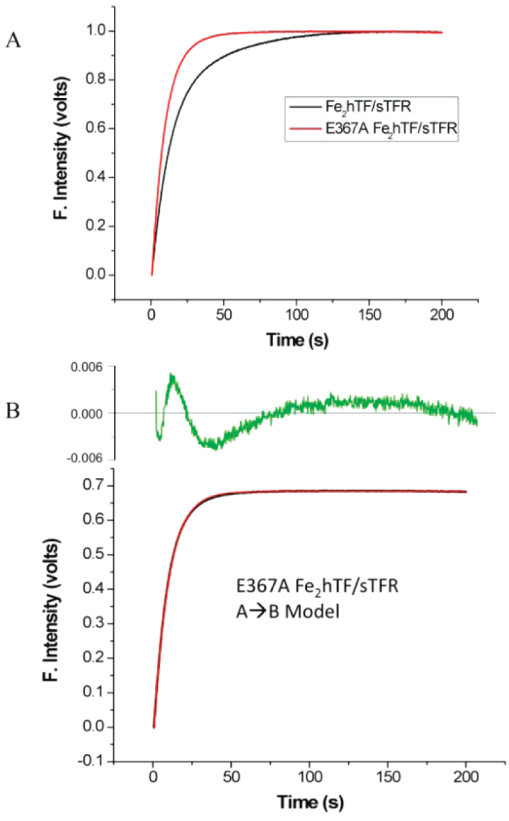

Figure 4. Release of iron from the Fe_2hTF–sTFR and E367A Fe_2hTF–sTFR complexes. (A) Overlay of iron release progress curves from the Fe_2hTF–sTFR (black) and E367A Fe_2hTF–sTFR (red) complexes. (B) Release of iron from the E367A Fe_2hTF–sTFR complex (black) fits best to a simple A → B model (red). Residuals are colored green. Attempts to fit the data to alternative models were unsuccessful (Figure 3 of the Supporting Information). All hTF–sTFR samples (375 nM) in 300 mM KCl were rapidly mixed with 200 mM MES (pH 5.6), 300 mM KCl, and 8 mM EDTA and excited at 280 nm. Emission was monitored using a 320 nm cut-on filter.

Kinetic Analysis of the Release of Iron from Fe_ChTF Mutants (in the absence of the sTFR). To further investigate the role of the charged residues that had an effect in the Fe_2hTF background (Arg352, Asp356, Glu367, and Lys511), we substituted them with alanine in the monoferric Fe_ChTF background (incapable of binding iron in the N-lobe). Rate constants for the release of iron from these mutants in the Fe_ChTF background under our standard conditions in the absence of the sTFR are presented in Table 2 of the Supporting Information. Two kinetic rate constants are obtained from fitting the Fe_ChTF data. Previously, we have shown that the first slow rate corresponds to the release of iron from the Fe_ChTF control, followed by a slightly faster conformational change.[11] Again, as expected in the absence of the sTFR, no major differences were observed in the rates of iron release between the Fe_ChTF control and the charged residue-to-alanine hTF, although the rate of conformational change was reduced by 20−40% for three of the four mutants (Table 2 and Figure 4 of the Supporting Information).

Formation of the D356A Fe_ChTF−sTFR Complex. As described, hTF−sTFR complexes were prepared by adding excess hTF to the sTFR followed by passage over an S-300HR gel filtration column to separate any excess hTF. A significant shift in the elution profile was observed following passage of the D356A Fe_ChTF−sTFR complex over the column (Figure 5A of the Supporting Information, peak 1), indicative of a greater column retention time and suggestive of a complex with an M_r lower than those observed for all of the other complexes (e.g., the Fe_2hTF−sTFR complex). Given these results, we further explored the stoichiometry of the D356A Fe_ChTF−sTFR complex. On the basis of qualitative sodium dodecyl sulfate−polyacrylamide gel electrophoresis (SDS−PAGE) analysis of the Fe_2hTF−sTFR complex and the D356A Fe_ChTF−sTFR complex, it appears that the D356A Fe_ChTF mutant does not form the standard 2:2 (hTF:sTFR monomer) complex but rather appears to form a 1:2 complex (Figure 5B of the Supporting Information).

Kinetic Analysis of the Release of Iron from Fe_ChTF Mutants (in the presence of the sTFR). We have previously established that a rapid conformational change (k_1) precedes the release of iron from the Fe_ChTF−sTFR complex (k_{2C}).[11] Rate constants for the selected charged residue-to-alanine Fe_ChTF mutants in the presence of the sTFR are listed in Table 3. Neither rate constant was affected by the R352A mutation in the Fe_ChTF−sTFR complex. On the basis of SDS−PAGE analysis of the D356A Fe_ChTF−sTFR complex (Figure 5B of the Supporting Information), it is not surprising that this complex fits only to a single rate (A → B model) that is slightly slower than the initial conformational change observed in the Fe_ChTF−sTFR control complex (Figure 5A). Nevertheless, it is clear from urea gel analysis that iron is completely removed from the D356A Fe_ChTF−sTFR complex (Figure 5B). The E367A mutation caused both the conformational change and the rate of release of iron from the Fe_ChTF−sTFR complex to increase by ∼50% (Table 3), yet a small fraction of the E367A Fe_ChTF−sTFR complex appears to retain iron following a 5 min incubation with iron removal buffer (Figure 5B). Interestingly, the data for the K511A Fe_ChTF−sTFR complex yielded two rate constants that are identical ($k_1 = k_{2C}$ = 15.9 min^{-1}). Thus, the rate for the initial conformational change (k_1) is slowed ∼23%, and the rate of release of iron from the K511A Fe_ChTF−sTFR complex is increased ∼121%.

Table 3. Kinetics of Release of Iron from Selected Charged Residue-to-Alanine Mutants in Fe_ChTF Background in the Presence of the sTFR

	k_1 (min^{-1})	k_{2C} (min^{-1})
Fe_ChTF[a]	20.6 ± 1.2	7.2 ± 0.4
R352A Fe_ChTF	21.4 ± 2.4	6.6 ± 0.4
D356A Fe_ChTF	15.7 ± 1.0	–
E367A Fe_ChTF	29.9 ± 3.1	10.7 ± 0.5
K511A Fe_ChTF	15.9 ± 0.8	15.9 ± 0.8

[a]From ref 11.

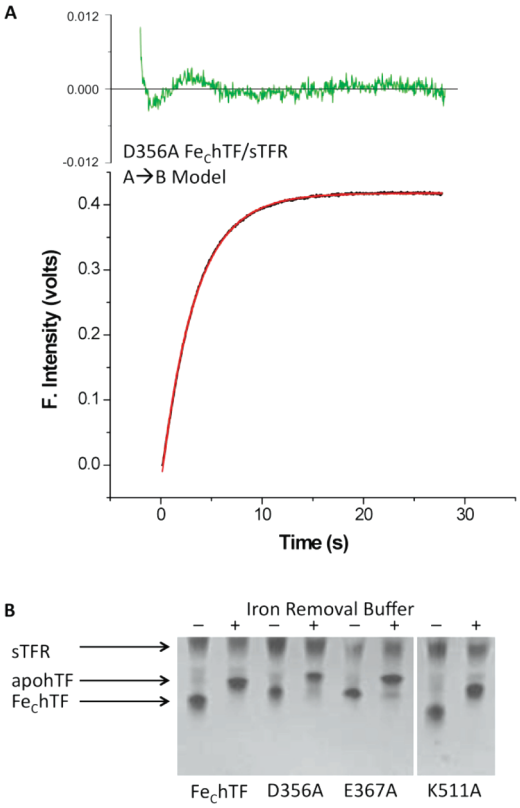

Figure 5. (A) Release of iron from the D356A Fe_ChTF−sTFR complex. The release of iron from the D356A Fe_ChTF−sTFR complex (black) fits to a simple A → B model (red). Residuals are colored green. The hTF−sTFR sample (375 nM) in 300 mM KCl was rapidly mixed with 200 mM MES (pH 5.6), 300 mM KCl, and 8 mM EDTA and excited at 280 nm. Emission was monitored using a 320 nm cut-on filter. (B) Urea gel analysis of selected charged residue-to-alanine Fe_ChTF mutants in the presence of the sTFR. Samples were electrophoresed before (−) and after (+) incubation with iron removal buffer [100 mM MES (pH 5.6) containing 300 mM KCl and 4 mM EDTA] for 5 min. Note the migration patterns of the charged residue-to-alanine mutants differ from that of Fe_ChTF because of differences in overall surface charge.

DISCUSSION

Overview. The interaction between hTF and the TFR is critical to cellular iron delivery in humans. Until recently, the molecular details of this protein−receptor interaction were obscure. Previous attempts to map the complex interaction between hTF and the TFR using in silico modeling[9] based on the cryo-EM model[8] suggested hTF−TFR interacting residues that required experimental verification. The recently determined crystal structure of the Fe_NhTF−sTFR complex (3.22

dx.doi.org/10.1021/bi201661g | Biochemistry 2012, 51, 686−694

Å)[10] has provided more precise information about the molecular interactions between hTF and the TFR. While the structure contributes significant insight, the mechanistic details of this dynamic and complex system cannot be completely elucidated by a crystal structure alone. Specifically, biochemical insights from the Fe_NhTF−sTFR complex structure are limited in a number of ways. For instance, given that the hTF in the complex crystal structure has iron bound only in the N-lobe and no density is observed for the C2 subdomain of hTF, it remains unclear whether the C2 subdomain has any effect on the binding of hTF to the TFR. It is possible that the contacts made between the C1 subdomain and the TFR may be strengthened or altered when iron is bound in that lobe. Importantly, the Fe_NhTF−sTFR crystals were grown and assessed at a pH similar to that of the blood where iron-bound hTF encounters the TFR (pH 7.5). Thus, the crystal structure cannot provide insight into how the interaction between hTF and the TFR changes as a result of a decrease in pH (from 7.5 to ∼5.6 in the endosome) or the release of iron from hTF (with accompanying large conformational changes within each lobe). For these reasons, we undertook biochemical studies of hTF residues putatively involved in the interaction between hTF and the TFR. Specifically, charged residues on the surface of hTF were chosen because of their potential to form strong intermolecular interactions through the formation of salt bridges, which provide substantial binding energy (∼4−5 kcal/mol).[17] In our study, 11 charged residue-to-alanine hTF mutants were analyzed for effects on iron release and binding to the sTFR to investigate the contribution of each of these hTF residues to the complex.

Asp356 Stabilizes the Iron-Bound hTF−sTFR Complex. In the Fe_NhTF−sTFR crystal structure, a salt bridge is clearly present between Asp356 of hTF and Arg651 of the TFR, as indicated by the short distance [2.7 Å (Figure 1D)] and the nearly continuous density between the two residues.[10] The current biochemical studies strongly support the importance of this interaction. It is clear that Asp356 of hTF is critical to the formation of a stable hTF−TFR complex, especially when iron is bound only in the C-lobe of hTF. Thus, the D356A Fe_2hTF mutant was unable to compete with biotinylated Fe_2hTF for binding to the sTFR in our assay (Figure 2); this result indicates that significant binding energy is provided by the Asp356−Arg651 salt bridge. This finding is consistent with the lower-molecular mass complex formed by the D356A Fe_ChTF mutant and the sTFR (Results and Figure 5 of the Supporting Information). Interestingly, and in stark contrast to >100 other hTF mutants we have studied, the D356A mutant in the monoferric C-lobe background does not appear to form the 2:2 (hTF:TFR monomer) complex and instead likely forms a 1:2 complex with the TFR. This finding suggests that cooperativity could exist; i.e., the binding of one iron-bound hTF molecule to the TFR dimer affects the binding of the second iron-bound hTF molecule. Moreover, the D356A mutation also affects the release of iron from the C-lobe of the Fe_2hTF−sTFR complex in which the rate constant is more than doubled (Table 2). This effect may be partially due to the proximity of Asp356 to His349, a residue previously shown to be absolutely critical to receptor-mediated release of iron from the C-lobe of hTF.[10,14] The absence of Asp356 would be expected to adversely affect the positioning of hTF α-helix 1 and thereby alter the interactions between His349 and the TFR. It is important to note that in the D356A Fe_ChTF−sTFR complex, only the first rate, corresponding to a conformational change in hTF, is observed (Table 3) with a rate constant of 15.7 min^{-1} compared to 20.6 min^{-1} for the Fe_ChTF−sTFR control complex (Table 3 and Figure 5A). We suggest that the iron release event following the rate-limiting conformational change is so fast that it cannot be observed because the urea gel indicates that the iron is completely removed from this construct (Figure 5B).

Glu367 Mediates Lobe−Lobe Communication in the Fe_2hTF−sTFR Complex. Although Glu367 was previously proposed to be involved in a salt bridge with Arg646 of the TFR by the in silico model,[9] which was based on the cryo-EM model,[8] the Fe_NhTF−sTFR crystal structure showed that Glu367 interacts not with Arg646 but rather with Phe650 of the TFR (Figure 1E). It is one of many van der Waals interactions between the C1 subdomain of hTF and the TFR.[10] This weak backbone−side chain (hTF−TFR) interaction would be maintained even in the E367A hTF mutant. However, the considerable effect of the E367A mutation on the binding of hTF to the TFR (Figure 2) suggests that Glu367 could be involved in an electrostatic interaction with the TFR when iron is bound in the C-lobe of hTF. Moreover, the effect of the E367A mutation on binding to the TFR emphasizes the importance of this interaction and the packing between α-helix 1 and β-strand 2 of hTF with αIII-1 and αIII-3 of the TFR helical domain. Significantly, αIII-3 of the TFR (on which both Arg646 and Phe650 are located) interacts not only with the C1 subdomain (including Glu367) but also with the N1 subdomain.[10] Curiously, the rate of release of iron from the C-lobe of the E367A Fe_2hTF−sTFR complex is increased by 20% (from 5.5 to 6.6 min^{-1}), while release of iron from the N-lobe is slowed drastically) (Figure 3 and Table 2). However, if there is no iron in the N-lobe, as is the case in the Fe_ChTF−sTFR complex, the E367A mutation increases the rate constants for the conformational change and release of iron from the C-lobe by 45 and 49%, respectively (Table 3). This finding suggests communication between the N- and C-lobes of hTF in the receptor complex that is potentially mediated through αIII-3 of the TFR with which the N1 and C1 subdomains of hTF interact.[10] We propose that the interaction of Glu367 may be very transient or changes significantly during the release of iron from the C-lobe of the hTF−TFR complex and that these changes are communicated to the N1 subdomain of hTF via αIII-3 of the TFR or vice versa. Intriguingly, mutation of Arg50, in the N1 subdomain of hTF, which is known to form a salt bridge with Glu664 of the TFR (located in a loop immediately following αIII-3) (Figure 1A), not only has a significant effect on binding to the TFR (Figure 4) but also slightly decreases the rate of release of iron from the C-lobe of the Fe_2hTF−sTFR complex by 29% [from 5.5 to 3.9 min^{-1} (Table 2)], possibly through a similar mechanism.

Lys511 Stabilizes the Iron-Bound C-Lobe in the hTF−sTFR Complex. Interactions proposed between the C2 subdomain of hTF and the TFR are especially intriguing because none were revealed by the cryo-EM model or the Fe_NhTF−sTFR crystal structure (which lacks any electron density for the C2 subdomain). Therefore, somewhat surprising is our finding that the K511A mutation in the C2 subdomain significantly affects the ability of the mutant to compete with Fe_2hTF for binding to the TFR (Figure 2). In the Fe_2hTF−TFR model, Sakajiri et al.[9] suggested that Lys511 could potentially interact, in conjunction with His349 in the iron-bound C-lobe of hTF, with Glu759 on the C-terminus of the TFR. Additionally, mutation of Lys511 to alanine significantly

increases the rate of release of iron from the C-lobe of hTF in the presence of the sTFR (Tables 2 and 3). Again, it has been previously shown that His349 acts as a histidine switch in the hTF−TFR complex to stimulate release of iron from the C-lobe of the complex.[10,14] It remains unclear from the data cited above whether Lys511 in the C2 subdomain has these effects by interacting with His349 in the C1 subdomain of hTF or by interacting with the TFR itself. However, it is clear from these findings that whatever interaction formed by Lys511 serves to stabilize the iron-bound C-lobe in the hTF−sTFR complex and prevent premature release of iron from the C-lobe.

Of the remaining charged residue-to-alanine hTF mutants tested in this study, mutation of Arg352 and Glu357 had significant effects on competitive binding of Fe_2hTF to the sTFR (Figure 2), and on the rate of release of iron from these mutants (Table 2). In Fe_NhTF, Glu357 is involved in relatively weak van der Waals interactions with Tyr643 of the TFR (Figure 1D), while Arg352 is more than 5 Å from any TFR residue in the Fe_NhTF−sTFR complex crystal structure (Figure 1C).[10] However, as mentioned above, the involvement of either Glu357 or Arg352 in alternative electrostatic interactions cannot be ruled out when iron is bound in the C-lobe of hTF. Also, given their proximity to other critical residues, (both Arg352 and Glu357 are located on α-helix 1 of the C1 subdomain along with key residues His349 and Asp356), it is not too surprising that these mutations affect binding of hTF to the sTFR. Likewise, the E141A and K148A mutations in the N2 subdomain of hTF had some effect on the binding of hTF to the TFR (Figure 2), but no effect on iron release (Table 2). Previous studies have shown that a loop sandwiched between these residues [Pro142-Arg143-Lys144-Pro145, also known as the PRKP loop (Figure 1B)] is critical for high-affinity binding of the N-lobe of hTF to the sTFR.[5] Hence, mutation of either Glu141 or Lys148 could affect the positioning of this important PRKP loop and thus have an impact on binding. In the C-lobe, mutation of residue Glu385 (that was only proposed to interact with the TFR in the in silico modeling study of Sakajiri et al.[9]) does have some effect on the binding to the sTFR (Figure 2) and slows the rate of release of iron, particularly from the C-lobe (Table 2). As Glu385, found on α-helix 3 of the C1 subdomain, does not interact with the TFR in the Fe_NhTF−sTFR crystal structure and is not located near any other known TFR-interacting hTF residues (Figure 1F), it remains unclear how mutation of this residue affects binding and the kinetics of iron release. Although the E357A/E625A mutant does affect the binding of hTF to the TFR, the effect is only slightly stronger than the effect caused by the E357A mutation alone; i.e., the E625A mutation has very little effect on binding. The two other hTF residues, Glu333 and Glu625, suggested by the in silico model of Sakajiri et al., to interact with the TFR have no effect on binding or iron release.

In summary, this work with charged residue-to-alanine mutants of hTF has revealed interesting features of the hTF−sTFR interaction. The detailed biochemical characterization reveals a number of intricate details that structural modeling studies have not provided to date. While the majority of the charged residue-to-alanine mutants presented in this study had some effect on the binding of hTF to the TFR, they are also likely involved in more subtle (nonionic) interactions with the TFR.

■ ASSOCIATED CONTENT

Supporting Information

Ribbon representation of the Fe_NhTF−sTFR crystal structure showing the location of the charged hTF residues mutated in this study, rate constants for release of iron from Fe_2hTF and Fe_ChTF mutants in the absence of the sTFR, urea gel analysis of selected charged residue-to-alanine mutants in the Fe_2hTF and Fe_ChTF backgrounds, alternative attempts to fit the E367A Fe_2hTF−sTFR complex iron release data, and a gel filtration profile and SDS−PAGE analysis of the D356A Fe_ChTF−sTFR complex. This material is available free of charge via the Internet at http://pubs.acs.org.

■ AUTHOR INFORMATION

Corresponding Author

*Department of Biochemistry, University of Vermont, Burlington, VT 05405. Telephone: (802) 656-0343. Fax: (802) 862-8229. E-mail: anne.mason@uvm.edu.

Present Address

‖Department of Genetics and Complex Diseases, Harvard School of Public Health, 655 Huntington Ave., Boston, MA 02115.

Funding

This work was supported by U.S. Public Health Service Grant R01 DK 21739 to A.B.M. and National Institute of General Medical Sciences Grant R37-GM-20194 to N.D.C. Support for A.N.S. and S.L.B. was provided by Hemostasis and Thrombosis Training Grant 5T32HL007594, issued to Dr. K. G. Mann at the University of Vermont by the National Heart, Lung and Blood Institute. A.N.S. is currently funded by an American Heart Association Predoctoral Fellowship (10PRE4200010).

■ ABBREVIATIONS

hTF, human serum transferrin; TFR, transferrin receptor; EM, electron microscopy; Fe_NhTF, recombinant N-terminally hexa-His-tagged nonglycosylated monoferric hTF that binds iron only in the N-lobe (Y426F and Y517F mutations prevent iron binding in the C-lobe); sTFR, glycosylated N-terminally hexa-His-tagged soluble recombinant transferrin receptor (residues 121−760); MMCO, molecular mass cutoff; NTA, nitrilotriacetic acid; EDTA, ethylenediaminetetraacetic acid; TBE, tris(hydroxymethyl)aminomethane−borate−EDTA; TMB, 3,3′,5,5′-tetramethylbenzidine; Fe_2hTF, recombinant N-terminally hexa-His-tagged nonglycosylated diferric hTF; Fe_ChTF, recombinant N-terminally hexa-His-tagged nonglycosylated monoferric hTF that binds iron only in the C-lobe (Y95F and Y188F mutations prevent iron binding in the N-lobe); BHK, baby hamster kidney.

■ REFERENCES

(1) Williams, J., and Moreton, K. (1980) The distribution of iron between the metal-binding sites of transferrin human serum. *Biochem. J. 185*, 483−488.

(2) Huebers, H., Josephson, B., Huebers, E., Csiba, E., and Finch, C. (1981) Uptake and release of iron from human transferrin. *Proc. Natl. Acad. Sci. U.S.A. 78*, 2572−2576.

(3) Zak, O., and Aisen, P. (1986) Nonrandom distribution of iron in circulating human transferrin. *Blood 68*, 157−161.

(4) Lawrence, C. M., Ray, S., Babyonyshev, M., Galluser, R., Borhani, D. W., and Harrison, S. C. (1999) Crystal structure of the ectodomain of human transferrin receptor. *Science 286*, 779−782.

(5) Mason, A. B., Byrne, S. L., Everse, S. J., Roberts, S. E., Chasteen, N. D., Smith, V. C., Macgillivray, R. T., Kandemir, B., and Bou-

Abdallah, F. (2009) A loop in the N-lobe of human serum transferrin is critical for binding to the transferrin receptor as revealed by mutagenesis, isothermal titration calorimetry, and epitope mapping. *J. Mol. Recognit. 22*, 521−529.
(6) Wally, J., Halbrooks, P. J., Vonrhein, C., Rould, M. A., Everse, S. J., Mason, A. B., and Buchanan, S. K. (2006) The crystal structure of iron-free human serum transferrin provides insight into inter-lobe communication and receptor binding. *J. Biol. Chem. 281*, 24934−24944.
(7) Dautry-Varsat, A., Ciechanover, A., and Lodish, H. F. (1983) pH and the recycling of transferrin during receptor-mediated endocytosis. *Proc. Natl. Acad. Sci. U.S.A. 80*, 2258−2262.
(8) Cheng, Y., Zak, O., Aisen, P., Harrison, S. C., and Walz, T. (2004) Structure of the human transferrin receptor-transferrin complex. *Cell 116*, 565−576.
(9) Sakajiri, T., Yamamura, T., Kikuchi, T., and Yajima, H. (2009) Computational structure models of apo and diferric transferrin-transferrin receptor complexes. *Protein J. 28*, 407−414.
(10) Eckenroth, B. E., Steere, A. N., Chasteen, N. D., Everse, S. J., and Mason, A. B. (2011) How the binding of human transferrin primes the transferrin receptor potentiating iron release at endosomal pH. *Proc. Natl. Acad. Sci. U.S.A. 108*, 13089−13094.
(11) Byrne, S. L., Chasteen, N. D., Steere, A. N., and Mason, A. B. (2010) The unique kinetics of iron-release from transferrin: The role of receptor, lobe-lobe interactions and salt at endosomal pH. *J. Mol. Biol. 396*, 130−140.
(12) Giannetti, A. M., Snow, P. M., Zak, O., and Bjorkman, P. J. (2003) Mechanism for multiple ligand recognition by the human transferrin receptor. *PLoS Biol. 1*, 341−350.
(13) Mason, A. B., He, Q. Y., Halbrooks, P. J., Everse, S. J., Gumerov, D. R., Kaltashov, I. A., Smith, V. C., Hewitt, J., and MacGillivray, R. T. (2002) Differential effect of a His tag at the N- and C-termini: Functional studies with recombinant human serum transferrin. *Biochemistry 41*, 9448−9454.
(14) Steere, A. N., Byrne, S. L., Chasteen, N. D., Smith, V. C., MacGillivray, R. T., and Mason, A. B. (2010) Evidence that His349 acts as a pH-inducible switch to accelerate receptor-mediated iron release from the C-lobe of human transferrin. *J. Biol. Inorg. Chem. 15*, 1341−1352.
(15) Byrne, S. L., Leverence, R., Klein, J. S., Giannetti, A. M., Smith, V. C., MacGillivray, R. T., Kaltashov, I. A., and Mason, A. B. (2006) Effect of glycosylation on the function of a soluble, recombinant form of the transferrin receptor. *Biochemistry 45*, 6663−6673.
(16) Mason, A. B., He, Q. Y., Adams, T. E., Gumerov, D. R., Kaltashov, I. A., Nguyen, V., and MacGillivray, R. T. (2001) Expression, purification, and characterization of recombinant non-glycosylated human serum transferrin containing a C-terminal hexahistidine tag. *Protein Expression Purif. 23*, 142−150.
(17) Masunov, A., and Lazaridis, T. (2003) Potentials of mean force between ionizable amino acid side chains in water. *J. Am. Chem. Soc. 125*, 1722−1730.
(18) Delano, W. L. (2002) *The PyMOL Molecular Graphics System*, DeLano Scientific, San Carlos, CA.

■ NOTE ADDED AFTER ASAP PUBLICATION

This paper was published ASAP on January 6, 2012 with in correct measurements in the Discussion section. The corrected version was reposted on January 17, 2012.